

## SEVO ON THE GROUND: DESIGN OF A LABORATORY SOLAR SIMULATION IN SUPPORT OF THE *O/OREOS* MISSION

AMANDA M. COOK<sup>1</sup>, ANDREW L. MATTIODA<sup>1</sup>, RICHARD C. QUINN<sup>2</sup>, ANTONIO J. RICCO<sup>1</sup>, PASCALE EHRENFREUND<sup>3</sup>,  
NATHAN E. BRAMALL<sup>4</sup>, GIOVANNI MINELLI<sup>1</sup>, EMMETT QUIGLEY<sup>1</sup>, RYAN WALKER<sup>1</sup>, AND ROBERT WALKER<sup>1</sup>

<sup>1</sup> NASA Ames Research Center, Moffett Field, Mountain View, CA 94035, USA; [andrew.l.mattioda@nasa.gov](mailto:andrew.l.mattioda@nasa.gov)

<sup>2</sup> SETI Institute, Mountain View, CA 94043, USA

<sup>3</sup> Space Policy Institute, 1957 E Street, N.W., Suite 403, Washington, DC 20052, USA

<sup>4</sup> Los Gatos Research, Mountain View, CA 94041, USA

Received 2013 June 12; accepted 2013 December 11; published 2014 January 9

### ABSTRACT

This technical note describes a novel solar simulation experiment designed to mimic the solar radiation experienced by the *Organism/Organics Exposure to Orbital Stresses (O/OREOS)* nanosatellite in low-Earth orbit. Thin films of organic compounds within hermetically sealed sample cells (identical to the films and cells of the spaceflight mission) were exposed to simulated AM0 solar radiation in the laboratory for a total of 6 months, and monitored for spectral changes at two-week intervals. The laboratory experiment accurately simulated ultraviolet and visible solar irradiance to within 2% from 200–1000 nm and the Ly $\alpha$  (121.6 nm) emission line radiation to within 8%. Design and calibration parameters for the experiment are discussed in detail for this ground-based laboratory irradiation experiment, which was built as a complement to, and as scientific validation of, the *O/OREOS* SEVO experiment in space.

*Key words:* astrochemistry – instrumentation: miscellaneous – Sun: UV radiation – techniques: spectroscopic

*Online-only material:* color figures

### 1. INTRODUCTION

Chemical evolution of organic matter in the solar system and throughout the universe is strongly influenced by solar (stellar) radiation, particularly from the vacuum ultraviolet (VUV) spectral region. To better understand such processes, testing the photostability and photochemical alteration of organics in actual space environments provides a powerful tool to study VUV effects combined with other relevant parameters (particle radiation, reduced gravity, temperature). Space-based experiments are motivated in part by the established difficulty in accurately simulating the complete space environment, particularly full-spectrum solar radiation, in a laboratory setting (e.g., Guan et al. 2010; Ehrenfreund & Westall 2012).

The importance of space-based measurements notwithstanding, the wider range of experiments, parameter modifications, and analyses available in ground-based laboratories make it essential to include laboratory solar simulation studies as a complement to any space-based exposure experiment. Space/laboratory comparisons can provide insights to accelerate and enhance our understanding of the mechanisms controlling the evolution of organic material in space. Such comparisons can also point to the deficiencies of laboratory solar simulator exposure systems.

Previous experiments exploring space's combined environmental influences have provided insight into the stability, degradation, and evolution of organic samples in low-Earth orbit (LEO; e.g., Rettberg et al. 2004; Ehrenfreund et al. 2007; Cottin et al. 2008; Horneck et al. 2010; Guan et al. 2010; Olsson-Francis et al. 2010; Ehrenfreund & Westall 2012; Rabbow et al. 2012). In particular, experiments on the European Space Agency BIOPAN 6 mission measured the half-lives of many amino acids, urea, and HCN-based polymers (Guan et al. 2010). Space data for samples retrieved from the BIOPAN facility differed, however, from those derived from ground control experiments using VUV light sources, demonstrating the importance of LEO-based

measurements and indicating the need for additional experimental measurements to reconcile space/ground discrepancies.

While most previous space-based experiments (see above) characterized samples at two time points—immediately before and at the conclusion of extended space exposure—the Space Environment Viability of Organics (SEVO) experiment onboard the *Organism/Organics Exposure to Orbital Stresses (O/OREOS)* nanosatellite recently demonstrated a new space-based technology that enables in-situ, real-time analysis of the photostability of organics during exposure. The ability to monitor the time-dependent effects of UV, VUV, and ionizing radiation in space provides greater insight into the kinetic details of photochemical reactions (Mattioda et al. 2012; Cook et al. 2014).

#### 1.1. The *O/OREOS* Mission

The *O/OREOS* nanosatellite (Ehrenfreund et al. 2012) includes a 10 cm spacecraft “bus” cube and two 10 cm cube astrobiology experiments: SEVO (Bramall et al. 2012; Mattioda et al. 2012) and the SESLO (Nicholson et al. 2011). The mission, launched in 2010 November, was the first under the Astrobiology Small Payloads program. After 6 months in orbit at an altitude of 650 km and an inclination of 72°, the *O/OREOS* spacecraft completed a fully successful science and technology demonstration mission in 2011 May (Ehrenfreund et al. 2012); today, after more than 2 yr in orbit, it continues to telemeter health-and-status data back to the student-operated ground station at Santa Clara University (Kitts et al. 2011).

SEVO exposes four classes of thin-film organics deposited on MgF<sub>2</sub> windows and in contact with pre-determined microenvironments (i.e., substrates, headspace gases) in sealed sample cells to the space radiation environment in LEO (Bramall et al. 2012). Using the Sun as a light source, the sample cells rotate into a fiber optic path leading to a compact UV/visible spectrometer just under the sample carousel. Spectroscopic measurements of the samples were carried out daily to biweekly,

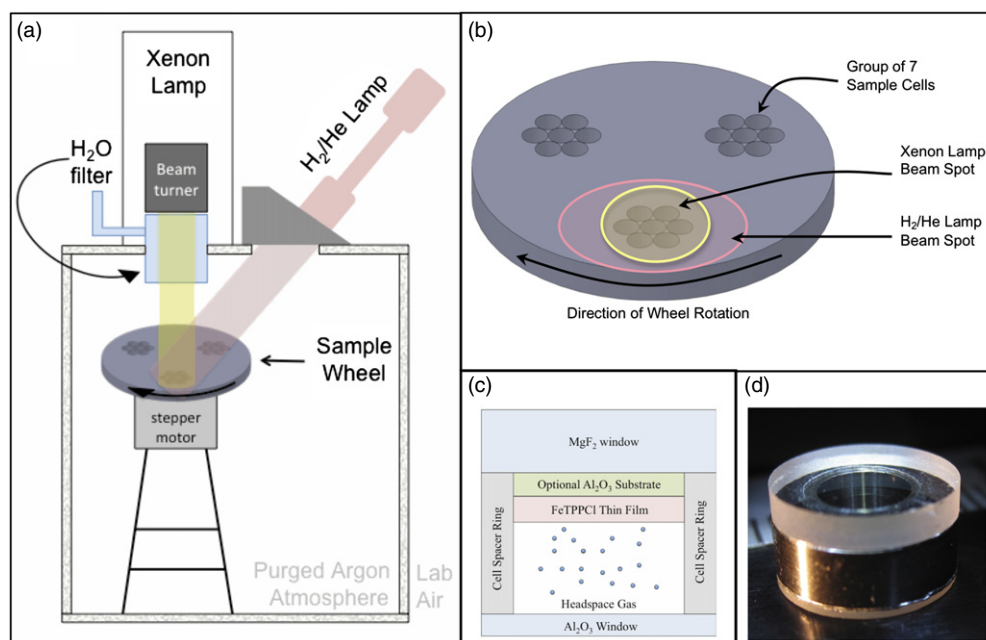


**Figure 1.** (a) Schematic of the solar simulation experiment inside an argon-purged glove box. Both lamps are mounted outside the glove box, with ports that allow radiation to pass through, intersecting at a group of sample cells on the sample wheel. The xenon lamp beam passes through a water filter to remove IR radiation before impinging on the samples. (b) A close-up schematic of the sample wheel, showing three groupings of seven sample cells. The xenon and H<sub>2</sub>/He lamp beams completely illuminate one group of the sample cells at a time. Each group remains in this position under the beams for 25 s before rotation of the wheel 120° to illuminate the next group; this cycle repeats continuously. (c) A schematic cross-section of a single SEVO sample cell, showing an organic thin film (in this case, FeTPPCL; see Table 1) in contact with a substrate and an enclosed headspace gas. (d) A photograph of one of the assembled SEVO sample cells.

(A color version of this figure is available in the online journal.)

depending on the mission phase, and telemetered back to Earth for analysis and interpretation. Significant changes were recorded in a number of the films in the SEVO experiment during flight; the changes were monitored as a function of time in orbit, from 2 weeks to 17 months, corresponding to as much as 3700 hr of direct solar exposure (Mattiola et al. 2012; Cook et al. 2014).

Here we report on the design of a ground-based laboratory irradiation experiment built as a complement to, and as scientific validation of, the SEVO experiment in space. The ground experiment exposes flight-duplicate SEVO samples simultaneously to two light sources that, in combination, simulate solar radiation. This technical note describes the design and calibration of the solar-simulation laboratory experiments used to simulate the *O/OREOS* nanosatellite radiation exposure parameters during the SEVO experiment. The goal is to highlight some important (and cost-effective) design and calibration techniques, so that other laboratories may continue to build on our approach for application to future LEO space exposure experiments. We also provide the technical details and experimental parameters that were used for interpretation of the SEVO flight data (Mattiola et al. 2012; Cook et al. 2014), which is now available to the science community upon request.

## 2. EXPERIMENTAL DESIGN

Figure 1 illustrates the main components of the experiment, the entirety of which was isolated in an argon-purged glove box. The glove box (Figure 1(a)) contained a platform to position a rotating “wheel” (Figure 1(b)) of sample cells at the appropriate height with respect to each light source. Two light sources, a xenon lamp and a H<sub>2</sub>/He microwave discharge lamp, were mounted on the outside surface of the glove box. The light sources were connected directly into the box using hermetically

sealed ports that allowed the light beams to intersect at the target samples on the wheel. The xenon lamp beam passed through a water filter before impinging on the samples, removing infrared radiation to prevent overheating of samples.

### 2.1. Sample Wheel

A schematic of the sample wheel design is shown in Figure 1(b). Sample cells (described below) were positioned in groups of seven in the aluminum wheel designed to secure them in bored-hole pockets. The configuration of the sample cells was chosen so that the largest number of cells would fit within the beam spot sizes projected by both lamps while maintaining uniform radiation exposure.

The sample wheel was mounted on a timed stepper motor (see Figure 1(a)), which rotated another set of samples (120° rotation) into the path of the intersecting lamp beams every 25 s. The rotation rate of samples in and out of the radiation beams approximated the stabilized rotation rate of the *O/OREOS* satellite (~1 rpm) in LEO, where samples were periodically shadowed from the Sun. The rotating wheel of sample cells was continuously exposed to simulated solar radiation for 6 months, with short breaks (usually <1 hr) for spectroscopic measurements.

In comparing the light exposure of the cells in the ground-based experiment with the SEVO spaceflight experiment, it is important to note that the direction of the Sun relative to the rotating satellite—which is passively oriented by magnetic rods to provide approximate alignment of its long axis with the local geomagnetic field lines—varied with the spacecraft’s position in any given 98 minute orbit and also with the orbital phasing details, which changed gradually over the course of the mission. Furthermore, during a variable fraction according to orbital phase (on average about one-third) of each individual

orbit, the nanosatellite was in solar eclipse, placing the samples in total darkness. Thus, the light/dark periods to which the spaceflight samples were exposed varied over the course of each orbit and over the duration of the mission as well, producing attendant variations in sample temperatures. The ground-based experiments therefore approximate one important aspect of the variations in solar illumination exposure to which the flight samples were subjected.

## 2.2. SEVO Sample Cells

Hermetically sealed sample cells (Figure 1(c)) with controlled initial gas composition, pressure, and substrate composition were used for the studies in LEO and in the laboratory simulation described here. Organic thin-film samples were prepared by subliming powdered solids directly onto  $\text{MgF}_2$  windows, or on top of inorganic substrates that were pre-deposited as thin films on the  $\text{MgF}_2$  windows. Detailed descriptions of the sample preparation have been published elsewhere (Bramall et al. 2012).

Two sets of samples were monitored for this experiment; their characteristics are tabulated in Table 1. The first was a set of control samples, which were housed in the purged glove box in a dark, light-tight container. The second set of sample cells were exposed in the solar-simulating irradiation experiment, housed in a rotating sample wheel, as described above.

## 2.3. Glove Box Environment

Dark control sample cells and irradiated sample cells were contained in a  $\sim 0.2 \text{ m}^3$  glove box (Figure 1) purged with inert argon gas. The argon environment protected the integrity of the organic sample films, reducing the possibility of other than inert gas leaking into the sealed cells (leak rates were measured for all sealed samples to be  $< 6 \times 10^{-10} \text{ mbar L s}^{-1}$ ). Argon pressure was maintained at just above 1 atm (Dual Purge<sup>TM</sup> system, Terra Universal, Fullerton, CA, USA). The purge control maintained a positive pressure of argon in the box via continuous low flow ( $\sim 63 \text{ cm}^3 \text{ s}^{-1}$ ), with intermittent high flow ( $> 70 \text{ cm}^3 \text{ s}^{-1}$ ) when pressure dropped in the box (e.g., when hands were removed from gloves, airlock was opened, etc.). At the low flow rate, the volume of gas contained by the glove box was replaced approximately every hour.

Atmospheric conditions in the box were monitored with a DewWatch humidity sensor (Terra Universal), which reported the dewpoint using a hygrometer placed at a central location inside the glove box. For the duration of the experiments, the dewpoint range was  $-70^\circ\text{C}$  to  $-30^\circ\text{C}$ , corresponding to 0.26–38 Pa water vapor pressure. At the ambient temperatures in the glove box ( $\sim 20^\circ\text{C}$ ), this amounts to a relative humidity of 0.2%–2%.

## 2.4. Xenon Arclamp

The majority of the solar spectrum from  $\sim 200 \text{ nm}$  to beyond  $2400 \text{ nm}$  was simulated with a 300 W xenon arclamp. However, the placement of the water filter in the beam path (to avoid sample heating) removes most of the flux above  $\sim 1000 \text{ nm}$  (Köfferlein et al. 1994). The arclamp power source was fitted with a UV-enhanced xenon bulb from Newport Corporation (part nos. 66485 and 6259), which provided flux down to  $\sim 200 \text{ nm}$ . The UV-enhanced lamp produced ozone, necessitating the use of a commercially available ozone scrubber to ensure laboratory safety and compliance with US federal health and safety standards.

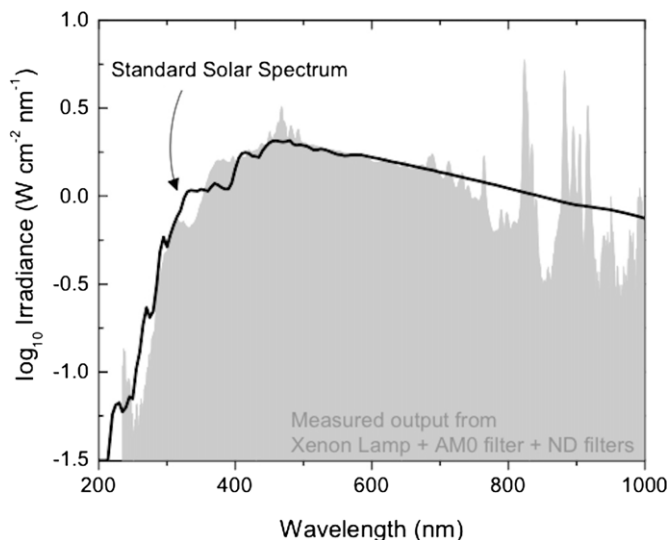


**Figure 2.** Solar irradiance spectrum (bold line), as measured in orbit at AM0 (Wehrli 1985), compared to the measured irradiance of our xenon lamp (gray area) through the water filter, AM0 filter, and neutral density filters. The integrated irradiance of the xenon lamp as measured from 200 to 1000 nm is within 2% of the integrated solar irradiance in the same wavelength range.

An AM0 filter was placed in the beam path to adjust the spectral irradiance from the xenon lamp. AM0 (air mass 0) is a term for the solar flux at Earth altitudes where there is no absorbance from intervening atmospheric material. The SEVO experiment aboard *O/OREOS* experienced AM0 solar flux at an altitude of 650 km in LEO; the goal of the laboratory simulation was to imitate this spectral irradiance.

To calibrate the lamp and in order to match the AM0 solar flux, the output from the lamp was measured at the position of the target samples. A series of neutral density filters was applied to coarsely reduce the flux and finer adjustments in intensity were made by adjustment of the current through xenon lamp.

Figure 2 compares the solar irradiance spectrum at AM0 (Wehrli 1985) to the calibrated output of the xenon arclamp, as measured by a laboratory UV/visible spectrometer. The integrated irradiance of the xenon lamp was within 2% of the integrated irradiance of the solar spectrum from 200–1000 nm. Although xenon lamps produce broadband, almost continuous emission at visible wavelengths, they do include a complex line spectrum in the 750–1000 nm region. Several lower-energy lines also exist around 475 nm. Between 400 and 700 nm,  $\sim 85\%$  of the total energy emitted by the xenon lamp resides in the continuum while  $\sim 15\%$  arises from the line spectrum. The xenon lamp output remains linear as a function of the applied current and can be adjusted to account for the decrease in output as the bulb ages. Bulbs were replaced when UV output (measured at  $\sim 220 \text{ nm}$ ) decreased by 25% or when the usage of the bulb exceeded 25% of the average lifetime ( $\sim 900 \text{ hr}$ , according to the bulb manufacturer).

## 2.5 Flowing $\text{H}_2/\text{He}$ Microwave Discharge Lamp

### 2.5.1 Overview

Photons from  $L\alpha$  hydrogen emission are expected to play a significant role in the processing of organic materials in space; many laboratory measurements on analog space materials are consistent with this theory (e.g. Gerakines et al. 2001; Bernstein

**Table 1**  
Sample Cell Characteristics for Laboratory Solar Simulation, Dark Control Experiments, and the Spaceflight Experiment

	Film Thickness	Microenvironment	Substrate	Number of Irradiated Samples (Approx. Percentage Photolyzed) <sup>a</sup>	Number of Dark Control Samples	Number of Spaceflight Samples
Isoviolanthrene (C <sub>34</sub> H <sub>18</sub> )	34 nm	Inert: 1 bar argon	MgF <sub>2</sub> window	1 (<5%)	1	1
		Surface: 1 bar argon	<10 nm SiO <sub>2</sub> film on MgF <sub>2</sub> window.	1 (<5%)	2	2
		Atmosphere: pCO <sub>2</sub> = 1000 Pa pO <sub>2</sub> = 1 Pa balance argon to 1 bar	200 nm Al <sub>2</sub> O <sub>3</sub> film on MgF <sub>2</sub> window	1 (<5%)	1	1
		Humid: 1 bar argon 0.8–2.3% relative humidity	200 nm Al <sub>2</sub> O <sub>3</sub> film on MgF <sub>2</sub> window	1 (30%)	1	1
Iron (III) tetraphenylporphyrin chloride (C <sub>44</sub> H <sub>28</sub> ClFeN <sub>4</sub> )	17 nm	Inert: 1 bar argon	MgF <sub>2</sub> window	1 (25%)	1	1
		Atmosphere: pCO <sub>2</sub> = 1000 Pa pO <sub>2</sub> = 1 Pa balance argon to 1 bar	200 nm Al <sub>2</sub> O <sub>3</sub> film on MgF <sub>2</sub> window	2 (10%)	2	2
		Humid: 1 bar argon 0.8%–2.3% relative humidity	200 nm Al <sub>2</sub> O <sub>3</sub> film on MgF <sub>2</sub> window	1 (100%)	1	2
Anthraruflin (C <sub>14</sub> H <sub>8</sub> O <sub>4</sub> )	79 nm	Inert: 1 bar argon	MgF <sub>2</sub> window	1 (<5%)	1	1
		Surface: 1 bar argon	<10 nm SiO <sub>2</sub> film on MgF <sub>2</sub> window.	1 (<5%)	1	
		Atmosphere: pCO <sub>2</sub> = 1000 Pa pO <sub>2</sub> = 1 Pa balance argon to 1 bar	200 nm Al <sub>2</sub> O <sub>3</sub> film on MgF <sub>2</sub> window	1 (<5%)	1	1
		Humid: 1 bar argon 0.8%–2.3% relative humidity	200 nm Al <sub>2</sub> O <sub>3</sub> film on MgF <sub>2</sub> window	1 (<5%)	1	1
L-Tryptophan (C <sub>11</sub> H <sub>12</sub> N <sub>2</sub> O <sub>2</sub> )	177 nm	Inert: 1 bar argon	MgF <sub>2</sub> window	1 (85%)	1	1
		Surface: 1 bar argon	<10 nm SiO <sub>2</sub> film on MgF <sub>2</sub> window.	1 (>90%)	1	1
		Atmosphere: pCO <sub>2</sub> = 1000 Pa pO <sub>2</sub> = 1 Pa balance argon to 1 bar	200 nm Al <sub>2</sub> O <sub>3</sub> film on MgF <sub>2</sub> window	2 (75%)	1	1
		Humid: 1 bar argon 0.8%–2.3% relative humidity	200 nm Al <sub>2</sub> O <sub>3</sub> film on MgF <sub>2</sub> window	1 (>90%)	1	1

**Note.** <sup>a</sup> Film changes measured as part of the laboratory solar simulation are reported (in parentheses) as an approximate percentage of the initial integrated absorbance lost (photolyzed) after ~1547 hr of total irradiation time.

et al. 2007; Guan et al. 2010). Historically and currently, many laboratory experiments have used microwave-discharge hydrogen flow lamps to simulate not just solar exposure, but also interstellar exposure (e.g., Allamandola et al. 1988; Gerakines et al. 2004; Cottin et al. 2003, 2008). The motivation for using such light sources has normally been their L $\alpha$  emission, because of its destructive effect on some of the most common molecules found in the interstellar medium (e.g., H<sub>2</sub>O, CO<sub>2</sub>, CO). It is essential to note, however, that significant variations in spectral output (i.e., relative to L $\alpha$  output) exist between very similar

hydrogen discharge lamp designs and operating parameters. For example, Samson (1967) showed that hydrogen discharge lamps become increasingly monochromatic sources (in L $\alpha$ ) as H<sub>2</sub> gas dilution increases. Similarly, Benilan et al. (2011) also determined that gas dilution results in greatly suppressed strengths from the otherwise strong (in pure H<sub>2</sub> gas flows) molecular H<sub>2</sub> bands centered at 160 nm. In the Benilan et al. (2011) study, the molecular bands were reduced to <4% of the L $\alpha$  emission line flux. Further, a study by Chen et al. (2011) indicated variation in spectral output due to the shape of the

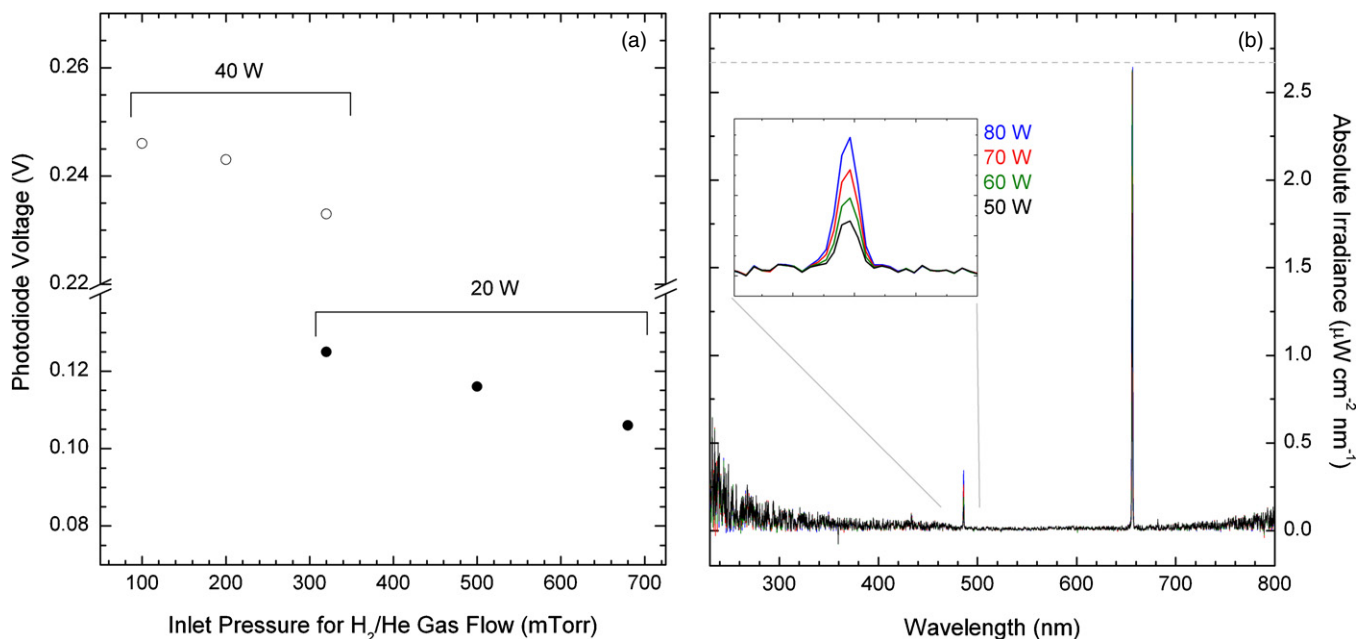


**Figure 3.** (a) Graph of the voltage produced by the VUV-sensitive photodiode in response to variations in microwave power and gas flow pressure for the H<sub>2</sub>/He discharge lamp. Note that decreases in power result in decreased flux detected (voltage produced) by the photodiode, while decreases in pressure result in increased flux detected by the photodiode. (b) UV/visible laboratory spectra of the H<sub>2</sub>/He lamp at increasing microwave powers (50–80 W). Note that the spectrum is flat where the spectrometer response is good (300–800 nm), with sharp Balmer emission lines superimposed. The inset shows one of the Balmer lines (486 nm, H $\beta$ ) increasing in strength as higher microwave powers are applied to the gas flow tube. The strongest Balmer line (656 nm, H $\alpha$ ) reached the saturation level of our spectrometer (marked by gray dashed line). See Section 2.5.3 for details.

(A color version of this figure is available in the online journal.)

flow tube, as well as with gas flow pressure, microwave power, and again, gas dilution ratios.

Therefore, to maximize simulation accuracy, solar/stellar radiation simulations require characterization and calibration of the individual light sources used in the laboratory. Comparison to the output of similar radiation sources, in lieu of direct calibration, is insufficient, since output has been shown to vary significantly (Chen et al. 2011), even under nominally similar operating parameters.

Since the energy of photon emission determines some aspects of its interaction with (or damage to) a molecule, it is important to understand the range of emission lines (and any continuum radiation) emanating from a laboratory irradiation source. Therefore, we measured and calibrated our source thoroughly. To properly calibrate the output from H<sub>2</sub>-discharge lamps, the ideal approach is to measure the VUV/UV (100–300 nm) spectrum of a given lamp used under known parameters of pressure, power, temperature, etc. This method requires access to a vacuum monochromator with sufficient resolution, and a vacuum (or inert atmosphere) container in which to measure the lamp's output, since laboratory air absorbs some of the radiation from these sources.

As a more affordable option for characterizing output from our H<sub>2</sub>/He discharge lamp, we used a commercially available VUV-sensitive photodiode to estimate photon fluxes. When such a photodiode is used in combination with and without a sapphire window, which filters wavelengths shorter than  $\sim$ 140 nm, it is possible to estimate the flux from the L $\alpha$  line. This method is described in the following subsections.

### 2.5.2. Implementation for this Experiment

A H<sub>2</sub>/He discharge lamp was included in the solar simulation experiment, to account for L $\alpha$  emission from the Sun at

AM0. The lamp hardware was similar to models described for simulations of interstellar ice irradiation (Gerakines et al. 2004; Cottin et al. 2003; Bouwman et al. 2011) and other solar simulation (Guan et al. 2010) experiments. Note that radiation from the lamp passed through a MgF<sub>2</sub> window before encountering the thin-film organic samples; the MgF<sub>2</sub> window is transparent down to  $\sim$ 110 nm.

For our lamp set-up, an H<sub>2</sub>/He gas mixture was flowed through a pyrex tube (12 mm diameter) surrounded by a McCarroll microwave cavity (Ophos Instruments). Gas flowed through the tube in a highly diluted mixture with helium (<1% partial pressure H<sub>2</sub>, balance He). The dilute mixture was achieved by attaching two gas cylinders—one pure He, and one 10% H<sub>2</sub>/He—to a line of tubing leading into the lamp and controlling the flows from both cylinders. A digital solid-state microwave generator (Ophos Instruments) was used to power the lamp; the generator provided power stability within 1% of the user-selected power.

Figure 3(a) plots the effect of power and pressure changes in the lamp. Several power and pressure settings were tested to identify trends in the behavior of the lamp. Figure 3(a) shows that increasing the power leads to higher lamp output, but that increasing the inlet pressure leads to lower lamp output. The output from the lamp was measured as the voltage response from a VUV-sensitive photodiode (International Radiation Detectors, Inc.; P/N AXUV100GLA, with current-to-voltage converter/amplifier; P/N AXUV100HYBV) placed at the location of the target samples. In general, the H<sub>2</sub>/He lamp flux was greater than necessary to simulate solar L $\alpha$ , so steps were taken to reduce the flux while maintaining stable intensity. After the voltage responses in Figure 3(a) were measured, a fine metal mesh filter was placed in the H<sub>2</sub>/He lamp beam path to reduce the flux reaching the target samples. Utilization of the mesh resulted in a  $\sim$ 70% reduction in flux,

as indicated by photodiode response, so the calibrated lamp produced voltages lower than what is shown in Figure 3(a). Microwave power was adjusted in 1 W increments for further fine-tuning.

For the optimized lamp settings, the flow of the 10% H<sub>2</sub>/He mixture was set for a pressure at the entrance of the vacuum-pumped lamp tube of 50 mtorr and the flow of pure He gas was adjusted until the pressure at the lamp entrance read a total of 730 mtorr. This resulted in a gas mixture with  $\sim 0.68\%$  H<sub>2</sub> (balance He) reaching the lamp. The flow rates, pressures, and lamp output typically stabilized  $\sim 20$  minutes after initializing these parameters.

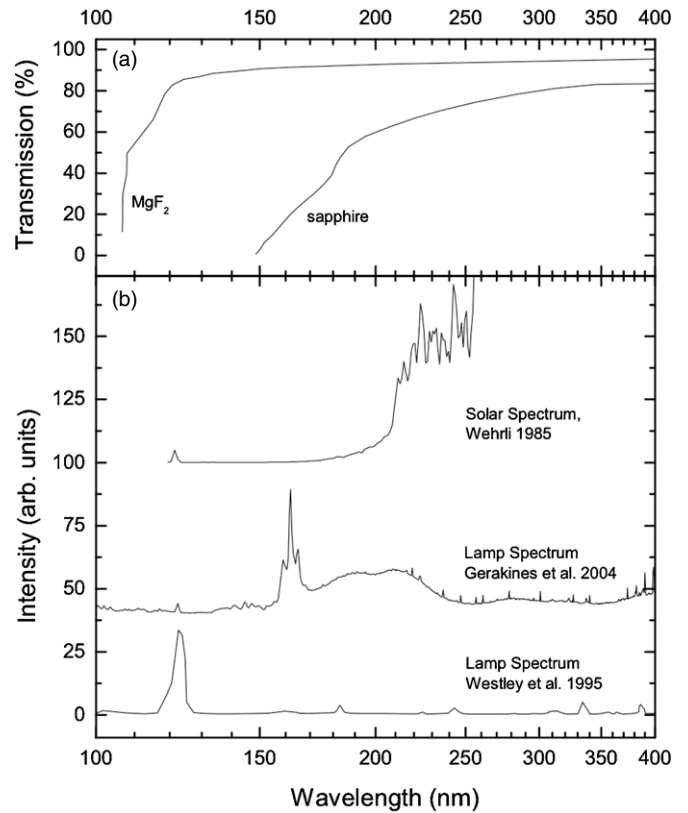
### 2.5.3 Calibration

Figure 3(b) plots the UV/vis spectrum of the lamp from 230–800 nm; the spectrum is reasonably flat, with sharp atomic emission lines superimposed. Strong Balmer lines (H $\beta$ , 486 nm; H $\alpha$ , 656 nm) are visible, but there are no broad lines and no discernable continua. The strength of the emission lines increased with increased microwave power applied at the flow tube; the inset of Figure 3(b) shows the increase of the H $\beta$  line as power increases from 50 to 80 W. The wavelength range of the UV/vis spectrometer did not permit direct measurement of any continuum radiation below 200 nm, nor the broad molecular H<sub>2</sub> lines at 160 nm (the latter being very common for pure H<sub>2</sub> lamps).

To mitigate the uncertainty in photon flux at shorter wavelengths, the broadband flux was measured with a VUV-sensitive photodiode detector. A 1 cm<sup>2</sup> photodiode with a directly deposited L $\alpha$  bandpass filter was placed at the position of our target samples. An appropriately designed VUV-enhanced photodiode without this bandpass filter responds to the entire range of 1–1000 nm photons. With the particular filter deposited on this photodiode, the responsivity outside the 116–135 nm range (L $\alpha$  is at 121.6 nm) is about four orders of magnitude weaker than without the filter; the response of the photodiode to the line is therefore enhanced relative to other wavelengths.

Two sets of measurements were taken with the filtered photodiode: one set with a sapphire window in the beam path, and one set without the sapphire window. The sapphire window was used to remove all photon flux at wavelengths below 140 nm. Thus, any flux detected by the photodiode with the sapphire window in place originated from wavelengths  $>140$  nm. Figure 4(a) illustrates the difference between the transmission of the sapphire window and the transmission when no sapphire window is used, and light is passing only through the MgF<sub>2</sub> window on the lamp itself. Figure 4(b) shows two previously published spectra from different H<sub>2</sub> lamps. Strong molecular H<sub>2</sub> bands are visible at 160 nm, while the L $\alpha$  line is much weaker, as reported by Gerakines et al. (2004). Conversely, the lamp spectrum from Westley et al. (1995) is dominated by L $\alpha$  emission. Note that the L $\alpha$  line falls exactly in the transmission window between sapphire and MgF<sub>2</sub>, as shown in Figure 4(b), and that this window also conveniently excludes any possible molecular emission at 160 nm.

The difference in the photodiode measurements with and without the sapphire window (accounting for Fresnel reflection off of the sapphire window), therefore, can be used to estimate what part of the total photon flux is  $<140$  nm. A significant majority of the flux  $<140$  nm comes from L $\alpha$ , based on previously published spectra (Westley et al. 1995; Samson 1980; Cottin et al. 2003).



**Figure 4.** (a) Transmission curve for MgF<sub>2</sub>, the window material used at the port of the flowing H<sub>2</sub>/He microwave discharge lamp, and for a 1 mm thick sapphire window that was placed over the photodiode detector for H<sub>2</sub>/He lamp calibration. (b) Plots showing relative intensity of the L $\alpha$  line for the solar spectrum, a pure H<sub>2</sub> discharge lamp (Gerakines et al. 2004), and another H<sub>2</sub> discharge lamp (Westley et al. 1995). Note that the strong molecular lines (160 nm) in the Gerakines et al. (2004) spectrum can be masked by the restrictive transmission curve of the sapphire window in panel (a). See Section 2.5.3 for detailed discussion.

The target L $\alpha$  photon flux was  $3.1 \times 10^{11}$  photons s<sup>-1</sup> cm<sup>-2</sup>, based on the average of orbital measurements of the solar flux at AMO (Vidal-Madjar 1975). The photon flux at the photodiode was calculated from the voltage produced by the photodiode, the resistance of the detector, and the responsivity of the photodiode as reported by the manufacturer. To achieve a L $\alpha$  dose close to that of solar L $\alpha$ , a measured voltage of  $\sim 12$  mV was desired. This was achieved by adjusting power and pressure until a voltage response of 50 mV was measured without the sapphire window in place, and 39 mV was measured with the sapphire window obscuring the detector. The difference between these two measurements, 11 mV, indicates the response of the detector from *only* those wavelengths below the sapphire cutoff (i.e., primarily L $\alpha$ ). By accounting for Fresnel reflection from the sapphire window ( $\sim 17\%$  of the light at the wavelength of interest), we determined that the total flux at wavelengths shorter than the sapphire window transmission cutoff yielded a voltage reading of 13.2 mV. This amounts to a L $\alpha$  photon flux of  $3.4 \times 10^{11}$  photons s<sup>-1</sup> cm<sup>-2</sup>, about 8% higher than that received from the Sun at AMO.

The lamp was typically run at a low power of 22–23 W. The lamp output remained stable over the six-month duration of the experiment; it was re-calibrated at three time points to make very minimal adjustments in intensity (modulating power by  $\pm 1$  W).

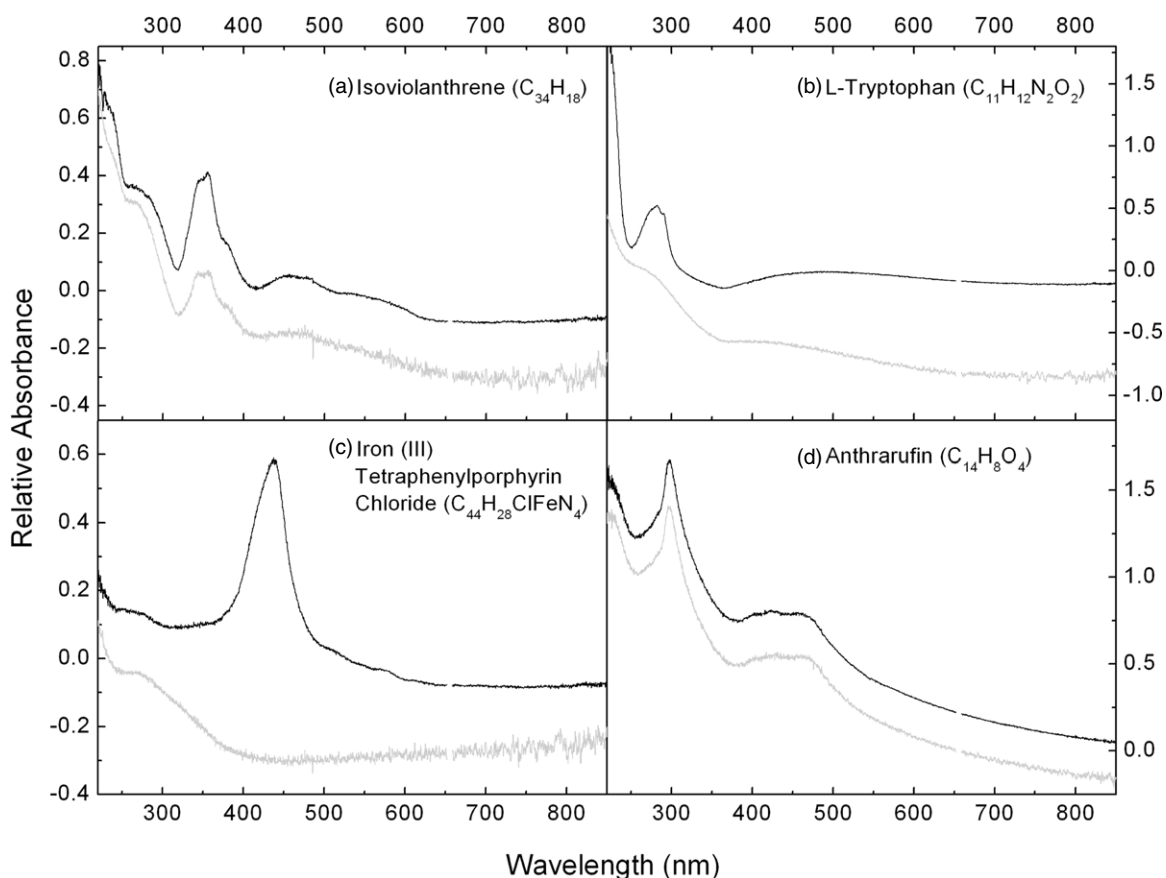


**Figure 5.** Selection of sample spectra measured before (black traces), and after (gray traces)  $\sim 1547$  hr of simulated solar irradiation. Black traces are vertically offset from gray traces for display. All spectra shown are from organic thin films contained in humid microenvironments (see Table 1). In general, humid cells displayed the most significant spectral changes over the course of the experiment. Other spectra, and scientific analyses are published in Mattioda et al. (2012) and Cook et al. (2014).

### 3. SAMPLE CELL MEASUREMENTS

Table 1 lists the samples that were included in the solar simulations and dark control experiments. Sample exposure to simulated solar radiation began 2012 May, and ended 2012 December, for a total of 4642 lamp hours. Accounting for sample wheel rotation, whereby cells were exposed for  $\sim 1/3$  of the total experiment time, each cell received  $\sim 1547$  hr of simulated solar exposure.

#### 3.1. UV/Visible Measurements

The absorbance spectra of sample cells exposed to simulated solar irradiation were measured via UV/visible spectroscopy at two-week intervals throughout the duration of the 6 month experiment. The UV/visible spectrometer was a high-resolution model from Ocean Optics (HR4000), coupled to a dual deuterium/halogen light source, also from Ocean Optics (DH-2000). Sample stability and/or change were measured spectroscopically and characterized for all of our samples in each microenvironment.

Figure 5 shows four examples of UV/visible spectra collected for this laboratory study. Black traces are initial spectra from before the irradiation experiment and gray traces are spectra measured at the conclusion of the irradiation exposure. The black traces are vertically shifted from the gray traces for display. Only samples contained in the *humid* microenvironment (see Table 1 for microenvironment parameters) cells are shown, since they exhibited the largest spectral changes. Loss of the

main absorbance features is apparent in panels (a)–(c); panel (d) shows no loss of absorbance for anthrarufin, a particularly stable molecule under the conditions studied. The results, which are reported in greater detail in Mattioda et al. (2012) and Cook et al. (2014) show that the photochemical degradation of certain organics is more efficient in the low ( $\sim 2\%$ ) relative humidity environments represented by the *humid* cells, than in the *inert*, *surface*, or *atmosphere* microenvironments. We generally attribute this degradation to film interactions with hydroxyl radicals, which are formed by UV irradiation of water vapor in the *humid* cells. Table 1 summarizes all laboratory spectral changes in the column entitled “Irradiated Samples,” expressed as percent loss for the main absorption feature. More comprehensive data sets and detailed scientific analyses of these changes are published in Mattioda et al. (2012) and Cook et al. (2014).

Dark control samples were measured monthly; no significant UV/visible spectroscopic changes were detected in the dark control samples. Spectra from the dark controls and the solar simulation provided a basis for interpretation of spectra from the SEVO flight experiment on *O/OREOS*. These data and analyses are discussed in Mattioda et al. (2012) and Cook et al. (2014).

### 4. CONCLUSIONS

The SEVO flight experiment, a 10 cm cube onboard the *O/OREOS* nanosatellite mission, is the first space-based

laboratory experiment to measure spectroscopic changes in organic films in situ while the films are being exposed to the space environment in LEO. The laboratory study described in this technical note complements the SEVO flight experiment by mimicking solar radiation conditions and temporal exposure patterns from satellite rotation, as well as providing high-quality UV/visible spectra of the samples from a laboratory spectroscopy system. The experimental design we present represents a sophisticated ground simulation, allowing a best possible comparison to data taken in LEO.

We emphasize the importance of light source measurements and calibration, particularly for flowing H<sub>2</sub>/He microwave discharge lamps, but also with respect to xenon arc lamps as solar simulators. For our experiment, the majority of the solar spectrum from ~200 to 1000 nm was simulated by the xenon arc lamp, so that integrated spectral irradiance in that wavelength region was accurate within 2% of the integrated solar irradiance spectrum. To simulate solar L $\alpha$  emission, an H<sub>2</sub>/He lamp was calibrated to produce an output within 8% of the solar L $\alpha$  strength.

The solar simulation experiment produced spectroscopic changes in the thin-film organic samples that changed at different rates than the spectra downlinked in the SEVO flight data. These differences, explained in detail in Mattioda et al. (2012) and Cook et al. (2014), appear to arise primarily as a result of temporal temperature variations that occurred onboard the satellite that were not duplicated in the laboratory experiments (Cook et al. 2014). While the 1/3 time exposure cycle does mimic the rotation of the satellite itself, it does not include portions of the satellite's orbit around the Earth during which the satellite was shadowed from the Sun for much longer periods, nor does it include those orbital phases where the cells were in sunlight nearly 100% of the time. Lastly, in the laboratory, we made no attempt to simulate cosmic ray impacts, which may play a role in the degradation of organic samples.

The results of our laboratory investigations, together with data from flight (Mattioda et al. 2012; Cook et al. 2014), highlight the importance of conducting space and laboratory experiments concurrently on identical samples. Differences between space exposure and laboratory exposure have been noted before (Guan et al. 2010), and the corresponding differences in our work confirm that point. This note describes our method for improving and fine-tuning laboratory experiments simulating solar exposure of organics. Further developments of this method could include considerations for temperature trends in orbit,

variable temporal light exposure cycles, and potentially particle radiation.

The authors thank the NASA Astrobiology Small Payloads program for support and Greg Defouw for assisting with the initial design/engineering of the exposure cells. The authors also thank the NASA Astrobiology Institute, the NASA Postdoctoral Program administered by Oak Ridge Associated Universities through a contract with NASA, and the NASA Exobiology Program for additional support (proposal number 09-EXOB09-1030).

## REFERENCES

- Allamandola, L. J., Sandford, S. A., & Valero, G. J. 1988, *Icar*, **76**, 225
- Benilan, Y., Gazeau, M.-C., Es-Sebbar, E.-T., et al. 2011, in EPSC-DPS Joint Meeting, EPSC-DPS2011-1317
- Bernstein, M. P., Sandford, S. A., Mattioda, A. L., & Allamandola, L. J. 2007, *A&A*, **664**, 1264
- Bouwman, J., Mattioda, A. L., Linnartz, H., & Allamandola, L. J. 2011, *A&A*, **525**, A93
- Bramall, N. E., Quinn, R., Mattioda, A. L., et al. 2012, *P&SS*, **60**, 121
- Chen, Y.-J., Chu, C.-C., Lin, Y.-C., et al. 2011, *AdG*, **25**, 259
- Cook, A. M., Mattioda, A. L., Ricco, A. J., et al. 2014, *AsBio*, in press
- Cottin, H., Coll, P., Coscia, D., et al. 2008, *AdSpR*, **42**, 2019
- Cottin, H., Moore, M. H., & Bénilan, Y. 2003, *ApJ*, **590**, 874
- Ehrenfreund, P., Ricco, A. J., Squires, D., et al. 2012, *AcAu*, **93**, 501
- Ehrenfreund, P., Ruitkamp, R., Peeters, Z., et al. 2007, *P&SS*, **55**, 383
- Ehrenfreund, P., & Westall, F. 2012, in *Laboratory Science with Space Data*, ed. D. Beysens, L. Carotenuto, J. van Loon, & M. Zell (Berlin: Springer), 103
- Gerakines, P. A., Moore, M. H., & Hudson, R. L. 2001, *JGR*, **106**, 33381
- Gerakines, P. A., Moore, M. H., & Hudson, R. L. 2004, *Icar*, **170**, 202
- Guan, Y. Y., Fray, N., Coll, P., et al. 2010, *P&SS*, **58**, 1327
- Horneck, G., Klaus, D. M., & Mancinelli, R. L. 2010, *MMBR*, **74**, 121
- Kitts, C., Rasay, R., Bica, L., et al. 2011, in 25th Annual AIAA/USU Conference on Small Satellites (Logan, UT), SSC11-II-3
- Köfflerlein, M., Döhring, T., Payer, H. D., & Seidlitz, H. K. 1994, in *International Lighting in Controlled Environments Workshop* (NASA-CP-95-3309; Kennedy Space Center, FL: NASA)
- Mattioda, A. L., Cook, A. M., Ehrenfreund, P. E., et al. 2012, *AsBio*, **12**, 841
- Nicholson, W. L., Ricco, A. J., Mancinelli, R., et al. 2011, *AsBio*, **10**, 951
- Olsson-Francis, K., de la Torre, R., & Cockell, C. S. 2010, *AEEM*, **76**, 2115
- Rabbow, E., Rettberg, P., Barczyk, S., et al. 2012, *AsBio*, **12**, 374
- Rettberg, P., Rabbow, E., Panitz, C., & Horneck, G. 2004, *AdSpR*, **33**, 1294
- Samson, J. A. R. 1967, *Techniques of Vacuum Ultraviolet Spectroscopy* (Lincoln, NE: Pied Publications)
- Vidal-Madjar, A. 1975, *SoPh*, **40**, 69
- Wehrli, C. 1985, *Physikalisch-Meteorologisches Observatorium + World Radiation Center (PMO/WRC) Publication No. 615* (PMO/WRC: Davos Dorf, Switzerland)
- Westley, M. S., Baragiola, R. A., Johnson, R. E., & Baratta, G. A. 1995, *P&SS*, **43**, 1311